Monitoring Agricultural Drought in Ningxia Region of China Using Remote Sensing Data and Deep Learning Model

Khandakar Md Bappy [1], Ali Shahzad [2], Abdul Basit [3], Shawkat Ali [4], Hidayat Ullah [5], Muhammad Awais [6], Zakria Zaheen [7], Kalisa Wilson [8*], Jiahua Zhang [9*]
[1-9] Remote Sensing Information and Digital Earth Center, College of Computer Science and Technology, Qingdao University, Qingdao 266071, China

* Corresponding Author: **Kalisa Wilson, Jiahua Zhang**

Article Info

P-ISSN: 3051-3383
E-ISSN: 3051-3391
Volume: 06
Issue: 02
July - December 2025
Received: 03-09-2025
Accepted: 05-10-2025
Published: 04-11-2025
Page No: 49-63

Abstract
Agricultural drought is a critical hydroclimatic hazard that severely impacts environmental and socioeconomic conditions, particularly in arid and semi-arid regions of Ningxia, China. Timely and accurate monitoring of agricultural drought is essential for understanding its dynamics and informing effective drought management strategies. This study presents a deep learning-based technique to capture the complex, nonlinear relationships between drought inducing factors using multi-source remote sensing and meteorological data from 2001-2020. Vegetation indices, precipitation, and soil-related variables were incorporated as independent predictors in a Deep Feedforward Neural Network (DFNN), with the Soil Moisture Deficit Index (SMDI) serving as the dependent variable during the growing season (April–October). For comparative analysis, two widely used machine learning algorithms Extreme Gradient Boosting (XGBoost) and Gradient Boosting Machine (GBM) were also evaluated. The results demonstrate that the DFNN model significantly outperformed both XGBoost and GBM in predicting SMDI, effectively capturing the spatial and temporal variability of agricultural drought across the growing season. In particular, the Standardized Precipitation Evapotranspiration Index (SPEI-3), which reflects short- to medium-term climatic anomalies, was identified as the most influential predictor, explaining 21.17% of the variability in agricultural drought. Moreover, the DFNN model exhibited strong stability and generalization ability during cross-validation, achieving a coefficient of determination (R^2) of 0.96, an RMSE of 0.26, and an MSE of 0.07 during the training phase. Furthermore, the DFNN model provided comprehensive agricultural drought monitoring by generating consistent spatial patterns of SMDI, demonstrating its applicability for accurate drought monitoring.

DOI: https://doi.org/10.54660/IJAIET.2025.6.2.49-63

Keywords: Agricultural Drought, Deep Learning, Smdi, Ningxia, Remote Sensing

1. Introduction

Drought is widely recognized as a recurrent and persistent hydroclimatic phenomenon that exerts profound impacts on both human societies and natural ecosystems (H. Chen *et al*., 2018; Mishra & Singh, 2010) [5, 31]. Despite its frequent occurrence, drought remains one of the least understood natural hazards because of its complex onset, gradual development, and substantial spatiotemporal variability characteristics that are strongly influenced by global climate change (C. Li *et al*., 2021; Wilhite *et al*., 1985) [27, 50]. Typically initiated by prolonged precipitation deficits, droughts are commonly categorized into meteorological, hydrological, agricultural, and socioeconomic types, which are interrelated and may occur sequentially (Mishra & Singh, 2010; Quiring, 2009) [31, 37].

Of these, agricultural drought characterized by a critical soil-moisture deficit that affects crop growth is particularly significant because of its direct consequences for food security and rural livelihoods (H. Chen *et al*., 2018; Yan *et al*., 2022) [5, 52]. In recent decades, agricultural drought patterns in parts of northern China have shown notable changes in frequency, duration and spatial extent, often linked to warming and changing water availability and to human interventions such as irrigation expansion (Sun *et al*., 2023; Yan *et al*., 2022) [44, 52]. Ningxia, in northwest China, is especially vulnerable because of its arid to semi-arid climate, limited precipitation and constrained water resources (notably dependence on the Yellow River), (Sun *et al*., 2023) [44] making drought a major challenge for local agriculture and development (Shi *et al*., 2022; J. Yang *et al*., 2015) [42, 53]. The region lies on the ecologically sensitive edge of the Mu Us Sandy Land, where desertification and drought-related impacts have shaped land-use and vegetation dynamics (Z. Chen *et al*., 2022) [8]. Consequently, a systematic analysis of the occurrence, severity, and spatiotemporal evolution of agricultural drought in Ningxia is of substantial theoretical and practical importance, and can inform drought risk management, early warning systems, and sustainable agricultural planning under a changing climate (C. Li *et al*., 2021; Yan *et al*., 2022) [27, 52].

Over recent decades, Ningxia has experienced a clear intensification of agricultural drought, significantly reduced crop yields and threatening agricultural productivity. (Tan *et al*., 2015a) [46] used the SPI and SPEI indices to show a significant drying trend from 1972 to 2011, with increasing drought intensity and duration. (Fang *et al*., 2018a) [14] reported rising drought frequency and severity in study region from 1960 to 2016 while (H. Chen & Sun, 2015) [6] found that severe and extreme droughts have become more frequent across northern China. (P. Yang *et al*., 2023) [54] highlighted the escalating threat of agricultural drought in study, (X. Li *et al*., 2024) [28] projected that climate change would exacerbate the impact of drought on wheat production. (Meng *et al*., 2024) [30] noted prolonged droughts in the Yinchuan Plain, causing soil-moisture deficits and reduced yields. (J. Yang *et al*., 2015) [53] emphasized the vulnerability of the area's agricultural systems and the urgent need for adaptive strategies. Collectively, these studies demonstrate the growing challenge of agricultural drought in study region and the urgent need for sustainable management strategies to address this issue.

Accurate monitoring of drought, a complex phenomenon driven by the interplay of meteorological and ecological factors such as precipitation, temperature, and vegetation response, requires a multifaceted approach that transcends traditional single-index methods. Widely used meteorological indices, such as the SPI and SPEI, provide crucial temporal insight into precipitation deficits; however, their reliance on ground-based measurements limits their ability to resolve fine scale spatial patterns across large regions (Vicente-Serrano *et al*., 2010) [47]. Remote sensing mitigates this limitation by offering continuous spatiotemporal data, leading to the development of numerous satellite-derived indices (e.g., Vegetation Condition Index (VCI) and Temperature Condition Index (TCI)) that track vegetation health and other anomalies (Kogan, 1995a) [15]. However, a fundamental challenge persists, as these indices, whether meteorological or remote-sensing-based, typically capture only a single aspect of drought, often failing to represent its full complexity and leading to potential misestimation (AghaKouchak *et al*., 2015) [2]. The integration of multi-source indices has emerged as a superior strategy for characterizing drought conditions. Conventional data-driven models used for such integration, such as traditional regression, often fail to capture the nonlinear relationships within these datasets (Jiao *et al*., 2016) [23]. Deep neural networks (DNN) provide a more robust framework for extracting these complex relationships, thereby enhancing characterization accuracy (Reichstein *et al*., 2019; C. Shen, 2018) [38, 40]. This study employs a spatial deep learning approach to integrate multiple remote sensing indices (VCI, TCI, VHI, EDI, PAI, and PCI) with meteorological indices (SPI/SPEI at 3, 6, and 12-month scales) for developing a more precise and comprehensive model to monitor agricultural drought.

The study addresses the SMDI to characterize agricultural droughts in Ningxia. The SMDI was selected as the primary drought metric because it directly quantifies soil water content, which is a critical factor for vegetation growth and a key indicator of agricultural drought stress(Narasimhan & Srinivasan, 2005) [32]. The index is particularly suitable for this application as it effectively captures short-term dry spells and their cumulative impacts on crops, while also enabling spatial comparisons across different climatic zones within the region (Mishra & Singh, 2010) [31]. To model the complex relationships driving drought, a DFNN was implemented, with the SMDI serving as the dependent variable to develop a robust monitoring framework for agricultural drought in this study region. Deep learning (DL), a subset of machine learning (ML) characterized by algorithms with multiple processing layers, has revolutionized the ability to automatically learn hierarchical and discriminative features from complex datasets (Reichstein *et al*., 2019) [38]. The adoption of DL models in geoscience has accelerated, driven by increased computational power and the recognition of their superior performance in handling high-dimensional and nonlinear relationships inherent in Earth system data (Duan *et al*., 2025) [13]. This trend is part of the broader emergence of ML as a critical analytical tool across environmental and agricultural sciences (Gyaneshwar *et al*., 2023) [19]. Traditional ML approaches have laid a strong foundation in the domain of agricultural drought monitoring. Models such as support vector regression (SVR), random forest (RF), and GBM have been successfully employed to integrate multi-sensor indices for effective drought assessment across diverse climatic regions (Park *et al*., 2016) [34]. For instance, random forests have proven highly effective for monitoring grassland droughts using remote sensing data (Wang *et al*., 2022) [49]. The effectiveness of advanced ensemble and hybrid models, such as XGBoost and CNN–RF architectures, has also been demonstrated to surpass traditional statistical models for meteorological and agricultural drought prediction (Xu *et al*., 2023) [51]. Collectively, these developments underscore the transformative role of DL techniques in enhancing the precision and robustness of drought monitoring systems, offering significant potential for applications in study region where drought impacts agricultural productivity.

However, recent reviews have highlighted that deep learning methods often exceed the capabilities of these classical ML models for complex spatiotemporal forecasting tasks (Prodhan *et al*., 2022) [35]. Recent studies have directly applied deep learning to drought challenges. (R. Shen *et al*., 2019a) [41] constructed a drought monitoring model using

deep learning based on multi-source remote sensing data. The model showed high stability during cross-validation and a high correlation with ground observations, providing early validation of the approach. (Prodhan *et al*., 2021) [36] demonstrated the effectiveness of deep learning techniques for monitoring agricultural droughts across South Asia. Similarly, (Y.; Zhang *et al*., 2023) [61] employed convolutional long short-term memory (ConvLSTM) models to develop a comprehensive framework for assessing drought conditions in northwest China. More advanced approaches, such as the hybrid deep learning model proposed by (Hanadé Houmma *et al*., 2022) [20] for drought forecasting, show the continued evolution of these techniques. While these studies provide a valuable foundation, a research gap remains in developing tailored deep learning systems for specific arid regions across Ningxia, with an explicit focus on the agricultural growing season. This study aims to address this gap by proposing an agricultural drought monitoring system for this study region using a DFNN. The model innovates by integrating a comprehensive suite of explanatory variables, including precipitation, soil moisture, and vegetation indices, specifically aligned with the critical phases of the regional growing season. This temporal alignment with the growing season, rather than a generic calendar period, allows for a more physiologically relevant assessment of drought stress. To ensure a rigorous evaluation, the performance of the proposed DFNN model was benchmarked against two powerful state-of-the-art machine learning models: XGBoost and GBM. The primary objective of this study was to develop an integrated drought monitoring framework that incorporates precipitation, soil, and vegetation factors using a deep learning approach. Therefore, the main aim of this study is to address the following objective: i) To evaluate the predictive accuracy of a DFNN model for agricultural drought during the growing season in Ningxia, in comparison with established machine learning approaches (XGBoost and GBM); ii) To identify the most influential drought indices (EDI, PAI, PCI, SPI, SPEI, VCI, TCI, VHI) for predicting SMDI; iii) To apply the developed DFNN model to generate spatial distribution maps of SMDI for typical drought years, thereby assessing the spatiotemporal patterns of agricultural drought in study area from 2001 to 2020.

2. Materials and Methods

2.1. Study Area

The Ningxia Region (35°14′–39°23′N, 104°17′–107°39′E) occupies approximately 66,400 km² in the upper Yellow River basin of northwestern China and is bordered by Gansu, Shaanxi and Inner Mongolia, with the Yellow River crossing its northern plains (Britannica, [s.d.]) [4]. The region's terrain is heterogeneous comprising mountains, loess hills and broad plains, notably the Helan and Liupan ranges and the central Ningxia Plain with a general decline in elevation from southwest to northeast (Du *et al*., 2021; H.; Zhang *et al*., 2022) [11, 59]. The study area lies in a semi-arid to arid continental (mid-latitude steppe) climate under monsoonal influence; mean annual temperature is 8°C, summers are hot and winters cold, and annual precipitation rises toward the southern highlands and is concentrated in summer (Tan *et al*., 2015b; H. Zhang *et al*., 2022) [46, 59]. Potential evaporation and evapotranspiration markedly exceed precipitation, producing persistent water deficits and prolonged dry spells outside the wet season (Du *et al*., 2021; H.; Zhang *et al*., 2022) [11, 59]. Long-term meteorological and remote-sensing studies report increases in drought frequency, duration and severity since the late 20th century, and pronounced spatio-temporal variability in agricultural drought during 2001–2020 justifying the use of index- and remote-sensing-based monitoring in this study (Tan *et al*., 2015b; Zhao *et al*., 2022) [46, 62]. Fig. 1 shows the land surface data types of the study area, including cropland, forest, shrub, grassland, water, snow/ice, barren, impervious, and wetland.

2.2. Data

This study used remote sensing and meteorological data to calculate drought indices. A detailed description of the datasets is presented in Table 1.

2.2.1. MODIS Data

The Moderate Resolution Imaging Spectroradiometer (MODIS), aboard NASA Terra and Aqua satellites, provides multispectral, medium-resolution observations widely applied in terrestrial and climate studies (Justice *et al*., 2002) [4]. In this study, we used the MOD13Q1 version 6 vegetation indices product (16-day composites, 250 m spatial resolution) and the MOD11A2 version 6 Land Surface Temperature (LST) product (8-day composites, 1 km spatial resolution) to derive the Vegetation Condition Index (VCI) and Temperature Condition Index (TCI) for agricultural drought indices (Didan, 2015; Wan, 2015) [10, 48]. The MOD13Q1 dataset, generated from atmospherically corrected red and near infrared reflectance, supports global vegetation monitoring and assessment of photosynthetic activity. While the MOD11A2 product provides clear sky averaged daytime and nighttime LST values that capture land atmosphere energy exchanges (Wan, 2015) [48]. Both datasets were accessed NASA LAADS DAAC (https://ladsweb.modaps.eosdis.nasa.gov/, on 11 January 2025) covering study area from 2001-2020.

2.2.2. GLDAS NOAH Soil Moisture, ET& PET

The Global Land Data Assimilation System (GLDAS) provides physically based, high-resolution land surface fields by driving multiple land surface models (Noah, CLM, VIC) with satellite and in-situ forcing (Rodell *et al*., 2004) [39]. In this study, the GLDAS Noah L4 monthly product (GLDAS_NOAH025_M_2.1; 0.25° × 0.25°) was used to obtain monthly top-layer 0–10cm soil moisture (SM), evapotranspiration (ET), and potential evapotranspiration (PET) (Beguería, *et al*., 2014; Rodell *et al*., 2004) [3, 39]. SM data were utilized to calculate the Standardized Moisture Deficit Index (SMDI) for both temporal and spatial analyses. Specifically, the time-series SMDI was employed to assess temporal drought variability from 2001 to 2020, while spatial SMDI mapping was conducted to evaluate the spatial distribution of drought intensity across the study Region. Using the same GLDAS dataset for both temporal and spatial SMDI ensures consistency and enables statistically robust comparisons of drought patterns over time and space. ET and PET data from GLDAS were further employed to derive the Evaporative Drought Index (EDI) to characterize surface dryness and atmospheric water demand (Yao *et al*., 2010; L. Zhang *et al*., 2019) [55, 60]. All GLDAS data were downloaded from NASA GES DISC (https://ldas.gsfc.nasa.gov/gldas/; accessed 20 February 2025) from 2001-2020.

2.2.3. CSIC SPEI

The Standardized Precipitation Evapotranspiration Index (SPEI) is a multiscalar drought indicator that integrates monthly precipitation and potential evapotranspiration to represent climatic water balance and drought severity (Vicente-Serrano *et al*., 2010) [47]. We used the SPEIbase global database (CSIC/SPEI/2_10) provided by the Spanish National Research Council which supplies monthly SPEI fields at 0.5° spatial resolution (SPEI timescales 1–48 months) (Beguería *et al*., 2014; SPEIbase v2.10, [s.d.]) [3, 43]. In this present study, we have focused on SPEI-03, SPEI-6 and SPEI-12month to characterize short-, medium- and long-term drought influences on vegetation and hydrology period from 2001–2020. SPEI products were downloaded from the global SPEI databased website (https://spei.csic.es/, accessed on 18 March 2025) over the study area.

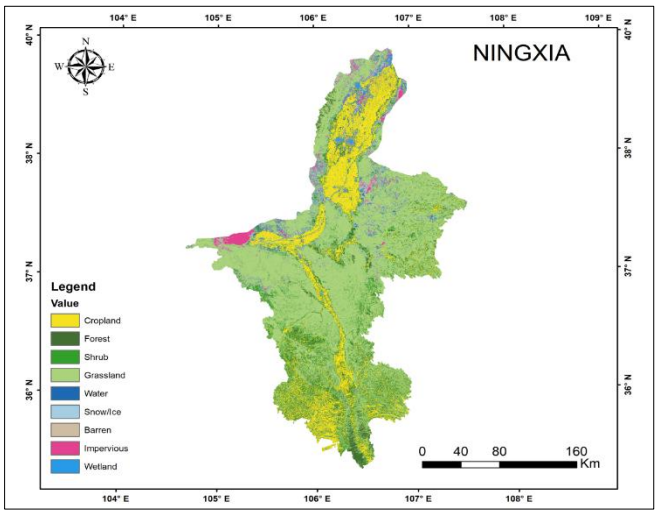

Fig 1: Land-use land cover (LULC) map for Ningxia.

Table 1: The Details of remote sensing data used this study.

Data Source	Data Type	Variables	Temporal Resolution	Spatial Resolution
MODIS	MODIS/061/MOD11A2	Land Surface Temperature (LST)	8 days	1km
	MODIS/006/MOD13Q1	Normalized Difference Vegetation Index (NDVI)	16 days	250m
CHRIPS	UCSB-CHG/CHIRPS/PENTAD	Precipitation	Monthly	5km
GLDAS NOAH	GLDAS_NOAH025_M_2.1	Soil Moisture (SM), Evapotranspiration (ET), And Potential Evapotranspiration (PET)	Monthly	0.25° × 0.25°
CSIC	CSIC/SPEI/2_10	Standardized Precipitation Evapotranspiration Index (SPEI)	Monthly	0.5° × 0.5°

2.2.4. CHIRPS

The Climate Hazards Group InfraRed Precipitation with Stations (CHIRPS) dataset provides a long, high-resolution quasi-global precipitation record (1981–present) that blends infrared satellite estimates with in-situ gauge climatologies to support drought monitoring and trend analysis (Funk *et al*., 2015) [17]. The CHIRPS monthly precipitation data aggregated from the CHIRPS daily/pentad collections (UCSB-CHG/CHIRPS) at 0.05° spatial resolution were utilized to compute precipitation-based drought Index. The datasets were downloaded from the Climate Hazard Center's website (https://www.chc.ucsb.edu/data/chirps/, accessed on 26 April 2025) from 2001–2020 period. These processed datasets were employed to derive the PCI, PAI, and SPI, which quantify both short and long-term precipitation variability. The extensive temporal coverage, gauge calibrated accuracy, and regional validation of CHIRPS make it particularly suitable for agricultural drought analysis in semi-arid regions of China (Gao *et al*., 2018) [18]. All the dataset was resampled to 1km spatial resolution using bilinear interpolation, and subsequently aggregated to represent the annual growing season.

2.3. Method

2.3.1. Modelling Methodology

Agricultural drought arises as a secondary consequence of meteorological drought, where extended precipitation shortages diminish soil moisture availability, thereby compromising crop productivity. The flowchart in Fig. 2 illustrates all procedures employed in this study for agricultural drought assessment, utilizing remote sensing data and model simulation outputs. Leveraging drought factors derived from multi-sensor remote sensing and meteorological data, we applied DFNN, XGBoost, and GBM to estimate the SMDI for analyzing drought conditions.

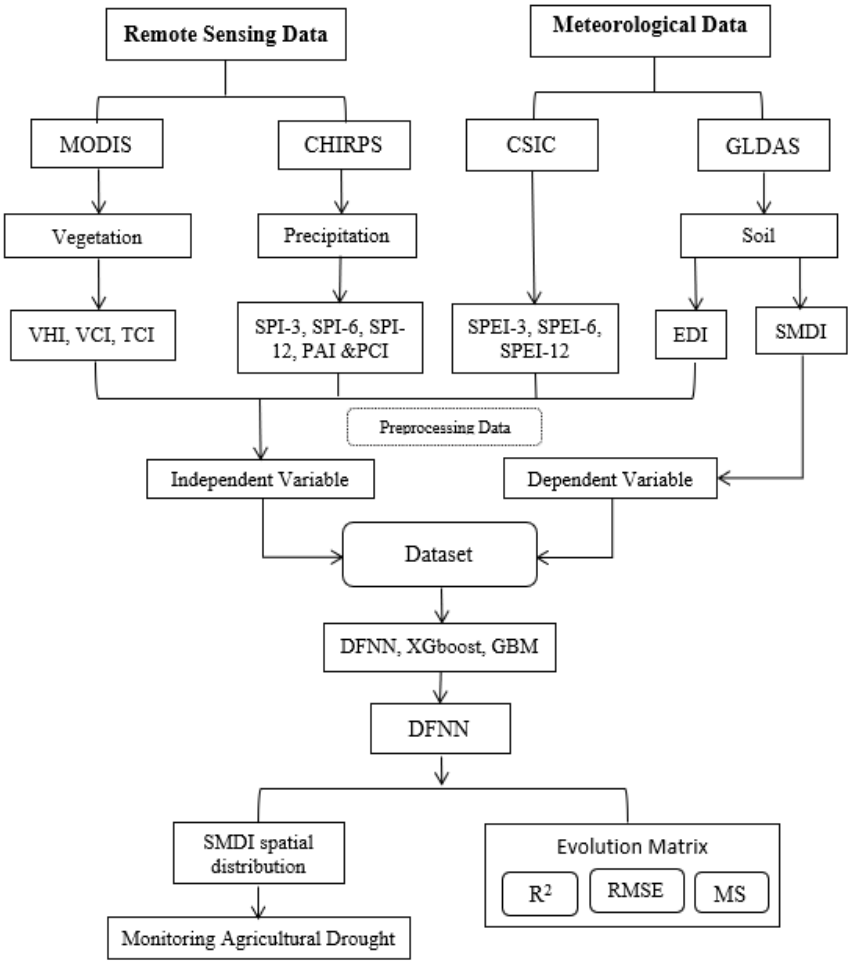

Fig 2: Methodological framework of this study.

The SMDI, a soil based agricultural drought indicator, was calculated using ground based observational data (soil moisture, precipitation, etc.) for the study region and served as the dependent variable in the model input. Subsequently, multisource remote sensing data including precipitation, vegetation indices, and soil moisture were processed through projection transformation, resampling, and clipping using ArcGIS, Python, Google Earth Engine (GEE), and R software. Focusing on the Ningxia region, three models were developed to estimate agricultural drought using remote sensing-derived drought factors: one deep learning approach DFNN and two machine learning approaches XGBoost and GBM. The optimal model was selected based on performance and stability evaluations. Using the best-performing model, the relative importance of each influencing factor was determined and compared with its Pearson correlation coefficient against SMDI. Finally, the selected model was applied to generate a spatial distribution map of drought in the study area, and the model estimated SMDI was used to assess drought conditions in typical.

2.3.2. Soil Moisture Drought Index (SMDI)

The SMDI is a standardized measure used to quantify deviations of soil moisture from long-term climatological conditions. Developed by (Narasimhan & Srinivasan, 2005) [32], it improves upon precipitation-based indices such as SPI and SPEI by directly representing soil moisture availability a critical factor influencing crop growth and drought stress. In this study, the SMDI was computed to evaluate agricultural drought conditions during the study period and used to characterize growing-season drought.

Calculation Procedure

The SMDI calculation consists of two steps: The SMDI computation involves two primary steps: (i) normalization of soil moisture anomalies, and (ii) recursive integration to account for temporal persistence of soil moisture. Normalization of soil moisture anomalies. For each month j, the soil moisture anomaly (SMj) is computed as:

$$SM_j = 100 \times \frac{SM_{\text{obs},j} - SM_{\text{med},j}}{SM_{\text{max},j} - SM_{\text{min},j}} \quad (1)$$

Where, $SM_{\text{obs},j}$ = Observed soil moisture (mm) for month j. $SM_{\text{med},j}$ = Long-term median soil moisture for month j. $SM_{\text{max},j}$ = Long-term maximum soil moisture for month j. $SM_{\text{min},j}$ = Long-term minimum soil moisture for month j. The normalization scales monthly anomalies to the range [-100, 100], effectively removing seasonality and allowing comparisons across months and years.

Recursive computation of SMDI. The first-month SMDI is initialized as:

$$\text{SMDI}_1 = \frac{\text{SM}_1}{50} \quad (2)$$

For subsequent months ($j \geq 2$), SMDI is calculated recursively to capture soil moisture persistence:

$$SMDI_j = 0.5 \times SMDI_{j-1} + \frac{SM_j}{50} \quad (3)$$

Here, $0.5 \times SMDI_{j-1}$ accounts for autocorrelation persistence of soil moisture. The divisor 50 scales the index to the range [-4, 4], making it consistent with Palmer-type drought indices.

Growing season Aggregation

Given that this study focuses on agricultural drought, the SMDI was aggregated over the regional growing season (April–October). Monthly SMDI values were first calculated for each month within this period and subsequently averaged to derive a single seasonal (annual) index value as follows:

$$SMDI_{\text{annual}} = \frac{1}{N} \sum_{j=\text{April}}^{\text{October}} SMDI_j, N = 7 \quad (4)$$

This aggregation provides a single annual SMDI value for each year, reflecting overall soil moisture deficits during the cropping period while retaining the persistence effects embedded in the monthly series.

Rationale for Monthly to Annual Approach

SMDI was computed sequentially on a monthly basis since its recursive formulation requires continuity between months. Calculating it directly from seasonal or annual means would overlook this temporal dependency and misrepresent drought dynamics. Long-term monthly climatologies ($SM_{\text{med},j}, SM_{\max,j}, SM_{\min,j}$) were derived over the study period record for each grid cell, and missing or inconsistent values were corrected using standard interpolation and quality-control procedures. The parameters used the persistence coefficient (0.5) and scaling factor (50). Negative SMDI values indicate below-normal soil moisture (drought), while positive values denote wetter-than-average conditions, providing a consistent and physically based measure of soil moisture variability across time and space.

Consequently, the SMDI was designated as the dependent variable in the DFNN model. A comprehensive description and methodological details of the SMDI are provided in (Narasimhan & Srinivasan, 2005) [32]. As outlined in their work, the SMDI for agricultural drought classification ranges from −4 to +4, as detailed in Table 2.

Table 2. SMDI Drought classification range based on (Narasimhan & Srinivasan, 2005) [32].

Drought Class	SMDI Range
Extreme Drought	-4 to -3
Severe Drought	-3 to -2
Moderate Drought	-2 to -1
Mild Drought	-1 to 0
No Drought	0 to 1

2.3. 3. Drought Construction formula

This study developed a comprehensive set of drought factors, with the SMDI and PCI calculated from GLDAS soil moisture and CHIRPS precipitation data, respectively, to characterize drought relevant to agricultural conditions (Funk *et al*., 2015; Rodell *et al*., 2004) [17, 39]. The PCI reflects precipitation anomalies and their persistence, while the SMDI quantifies cumulative soil deficits and serves as the primary indicator of agricultural drought severity. The TCI derived from MODIS LST highlights thermal anomalies associated with drought, with higher values indicating drier surface conditions. Evaporative stress was represented by the EDI, computed as the ratio of ET and PET from GLDAS; lower values signify intensified evaporative deficits and surface dryness. Meteorological drought was assessed using the PAI, SPI at 3-, 6-, and 12-month timescales, and SPEI 3-, 6-, and 12-month to capture precipitation deficits across multiple timescales (Mckee *et al*., 1993; Vicente-Serrano *et al*., 2010) [29, 47]. Vegetation responses were represented by the VCI and VHI, which reflect temporal deviations in vegetation condition attributable to moisture anomalies. The calculation formulas for all indices are presented in Table 3.

Table 3: Calculating formula for all types of variables use this study.

Drought Variable	Formula	Reference
EDI	$EDI = 1 - \frac{ET}{PET}$	(Yao *et al*., 2011) [55]
PAI	$PAI = \frac{P_i - \overline{P}}{\overline{P}} \times 100$	(R. Shen *et al*., 2019b) [41]
PCI	$PCI = \frac{P - P_{min}}{P_{max} - P_{min}} \times 100$	(A. Zhang *et al*., 2019) [58]
SPI	$SPI = K - \frac{c_0 + c_1 k + c_2 k^2}{1 + d_1 k + d_2 k + d_3 k^3}$	(Mckee *et al*., 1993) [29]
TCI	$TCI = \frac{LST_{max} - LST_i}{LST_{max} - LST_{min}} \times 100$	(Felix N. Kogan, 1997) [15]
VCI	$VCI = \frac{NDVI_i - NDVI_{min}}{NDVI_{max} - NDVI_{min}} \times 100$	(Kogan, 1995b) [25]
VHI	$VHI = \alpha VCI + (1 - \alpha)\, TCI$	(Kogan, 2000) [26]

2.4. Machine learning and Deep learning Approaches

2.4.1. XGBoost (Extreme Gradient Boosting)

XGBoost is a scalable machine learning system for gradient tree boosting that builds an ensemble of models in an additive, iterative manner to minimize a regularized objective function (T. Chen & Guestrin, 2016) [7]. While rooted in the principles of Gradient Boosting Machines (Friedman, 2001) [16]. XGBoost enhances the framework through several key innovations. Its core strength lies in the use of a second-order Taylor approximation of the loss function, which provides a more informative direction for model updates compared to first-order gradient descent alone. The model's objective at iteration t is formulated as:

$$obj^{(t)} = \sum_{i=1}^{n} l\left(\left(y_i, \hat{y}_i^{(t)}\right) + \Omega(f_t)\right) \quad (5)$$

Where, ℓ $(\cdot)$ is a differentiable convex loss function measuring the difference between the true label y_i and the prediction is $\hat{y}_i^{(t)}$. The term $\Omega(f_t)$ is a regularization component that penalizes the complexity of the tree ft, defined as: $\Omega(f) = \gamma T + \frac{1}{2}\lambda \|w\|^2$.

Here, T is the number of leaves in the tree, w is the vector of leaf weights, γ is a parameter that discourages creating additional leaves, and λ is the L2 regularization term on the weights. This regularized objective, combined with efficient algorithms for finding optimal tree structures and support for data subsampling (both row-wise and column-wise), effectively controls overfitting and improves computational performance. In this study, the performance of the XGBoost model was evaluated using the same cross-validation procedure, with performance assessed via R^2 and RMSE as the primary performance metrics.

2.4.2. GBM (Gradient Boosting Machine)

The Gradient Boosting Machine (GBM) is an ensemble learning method that constructs a predictive model in a stage-wise fashion by optimizing an arbitrary differentiable loss function (Friedman, 2001) [16]. In contrast to other advanced boosting algorithms that may employ second-order approximations, GBM relies on a gradient descent procedure to minimize the loss, providing a robust and conceptually straightforward approach. In this additive ensemble, base learners, typically regression trees, are sequentially fitted to the negative gradients (pseudo-residuals) of the loss function from the previous model. For a loss function $L\left(y, F(x)\right)$ the pseudo-residuals at iteration m are computed as: $r_{im} = -\left[\frac{\partial L(yi, F(x_i))}{\partial F(x_i)}\right]_{F(x)=F_{m-1}}$. The model is then updated by adding the new base learner, scaled by a learning rate ν:

$$F_m(x) = F_{m=1}(x) + v.\sum_{j=1}^{J_m} \gamma_{jm} I\left(x \in R_{jm}\right) \quad (6)$$

where γ_{jm} are leaf weights and r_{jm} are the terminal regions (leaves) of the tree. This gradient-descent boosting framework inherently incorporates regularization techniques such as shrinkage (via the learning rate) and stochastic subsampling of the data to improve generalization and mitigate overfitting. In this study, the GBM served as a comparative baseline, and its performance was evaluated using 5-fold cross-validation with the Mean Squared Error (MSE) as the performance metric.

2.4.3. Construction of deep learning model using DFNN

Deep learning approaches such as convolutional neural networks (CNN), recurrent neural networks (RNN), and deep feedforward neural networks (DFNN have been widely adopted in environmental and agricultural applications for their ability to capture nonlinear, high-dimensional relationships between climatic and biophysical variables (Ian Goodfellow *et al*., 2016; Prodhan *et al*., 2021) [22, 36]. In this study, DFNN Model was implemented in Python using the TensorFlow/Keras framework (Abadi *et al*., 2016; Chollet, 2015) [1, 9], to predict SMDI from twelve multi source predictors (precipitation, vegetation, and soil indices). The network comprised an input layer (12 features), three hidden layers with 312, 156 and 78 neurons, respectively, and a single-node output layer shown in Fig. 3; nonlinear activation functions were applied to hidden layers to facilitate the approximation of complex mappings.

In the present study, Total number of 130,000 samples were randomly selected and 80% of data used for training and 20% data used to the test set as for prior to training, all predictors were standardized to zero mean and unit variance. Model calibration involved systematic hyperparameter tuning (epochs, batch size, learning rate, regularization, and optimizer choice) using cross-validation and an independent validation subset drawn from the training set to guide selection and to reduce overfitting. Predictive performance was assessed on the held-out test set using standard metrics (R^2, RMSE and MSE) to provide an unbiased estimate of generalization; following validation, the optimized DFNN was applied to the entire dataset to generate continuous spatial and temporal drought predictions for comprehensive monitoring across the study period.

2.5. Accuracy Evaluation

This study, we enhanced the performance of the deep learning approach by identifying hyperparameters that affect model stability through a trial-and-error method. Optimal parameters for XGBoost, GBM, and DFNN were performed using 5-fold cross validation. hen, XGBoost, GBM and DFNN are validated with 80% and 20% of the datasets, respectively. The datasets were randomly selected into training and test sets, with this process repeated 100 times to evaluate the stability of each model. After that, Performance was evaluated using the coefficient of determination R^2, RMSE and MSE.

The coefficient of determination is given by:

$$R^2 = \frac{(\sum_{i=1}^{n}(O_i - \bar{O})(P_i - \bar{P}))^2}{\sqrt{\sum_{i=1}^{n}(O_i - \bar{O})^2}.\sqrt{\sum_{i=1}^{n}(P_i - \bar{P})^2}} \quad (8)$$

The Root Mean Square Error is expressed as:

$$\text{RMSE} = \sqrt{\frac{\sum_{i=1}^{n}(O_i - P_i)^2}{n}} \quad (9)$$

And the Mean Squared Error is defined as:

$$\text{MSE} = \frac{\sum_{i=1}^{n}(O_i - P_i)^2}{n} \quad (10)$$

Where n is the number of samples, O_i is the actual value, P_i is the predicted value, $\bar{O}$ is the mean of observed values, and $\bar{P}$ is the mean of predicted values, model performance is evaluated using these key metrics. A higher R2 value indicates a better model fit, while lower RMSE and MSE values suggest greater accuracy in predictions to identify the drought condition.

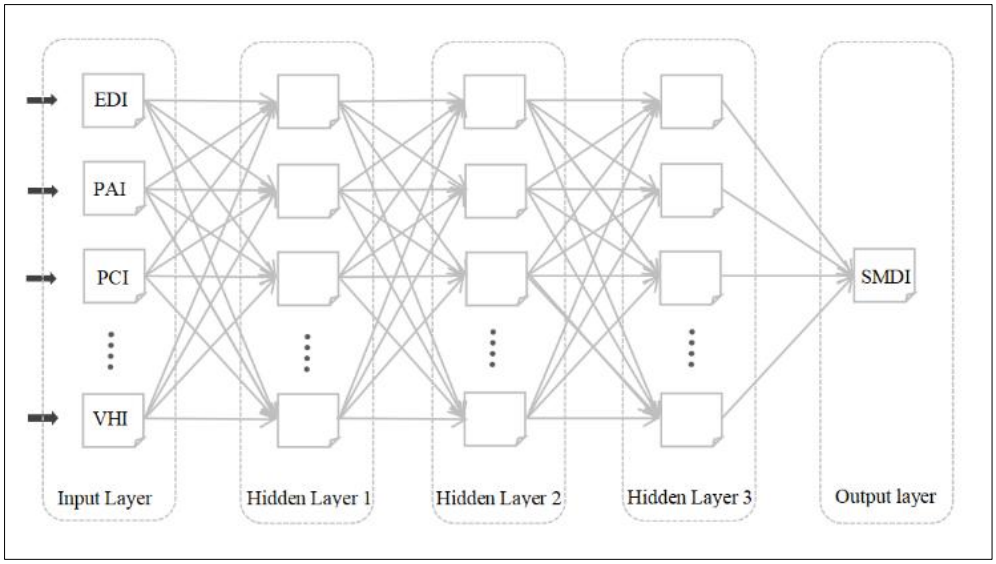

Fig 3: An architecture of the DFNN model used in this study with one input layer, three hidden layers, and a single output neuron predicting the SMDI.

Table 4: A selection of result scoring performance of DFNN model.

Layers	Neurons	Epochs	Train-R2	Train-RMSE	Train-MSE	Test-R2	Test-RMSE	Test-MSE
4	256-128-64	63	0.962	0.258	0.066	0.958	0.271	0.073
4	256-128-64	51	0.959	0.265	0.069	0.957	0.272	0.074
4	256-128-64	60	0.962	0.258	0.066	0.961	0.264	0.070
4	256-128-64	40	0.955	0.283	0.080	0.951	0.292	0.085
4	256-128-64	55	0.961	0.262	0.069	0.959	0.269	0.072

3. Results

3.1. Model Accuracy comparison

In this study, DFNN, XGBoost, and GBM models were developed using selected influencing variables to predict observed SMDI values. The optimal parameters for each algorithm were determined via 5-fold cross validation (see Table 5), after which their predictive performance was evaluated. The results indicate that the DFNN model achieved the highest accuracy in simulating SMDI, with its output closely aligning with the actual measurements, as illustrated in Figure 4. For the training set, DFNN attained an R^2 of 0.96 (RMSE = 0.26, MSE = 0.07), while on the test set, it sustained a robust performance with an R^2 of 0.95 (RMSE = 0.27, MSE = 0.07). In comparison, the XGBoost and GBM models demonstrated slightly lower accuracy, with test set R^2 values of 0.90 (RMSE = 0.40, MSE = 0.16) and 0.92 (RMSE = 0.37, MSE = 0.16), respectively.

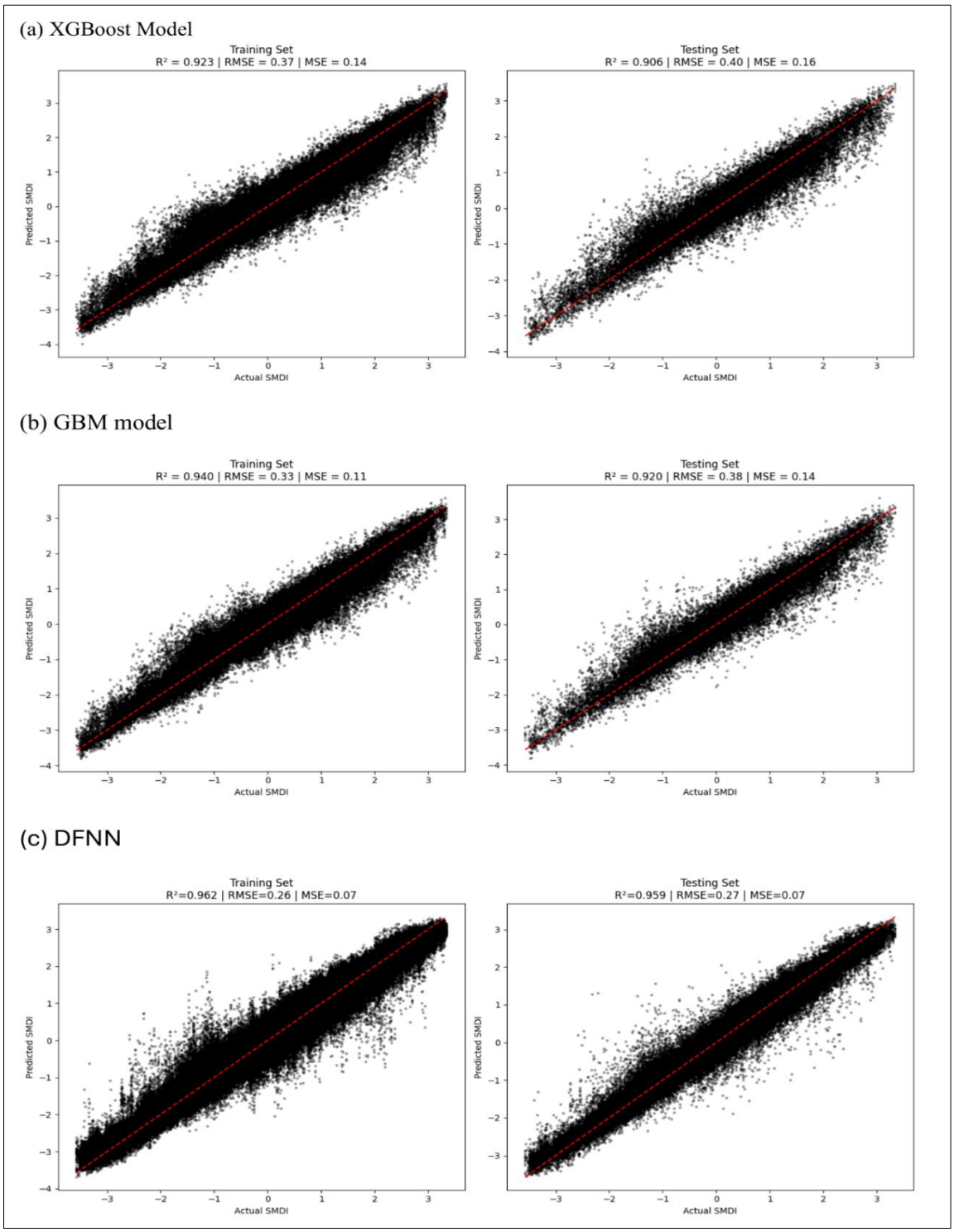

Fig 4: Comparison of the predicted and actual SMDI scatterplot with the (a) XGboost, (b) GBM and (c) DFNN models for the training and test sets.

Table 5: The details list of parameters with their value used for XGBoost, GBM and DFNN.

Model	Parameters
XGboost	n_estimators (150), learning_rate (0.2), max_depth (6), subsample (0.8), colsample_bytree (0.8), reg_alpha (0.1), reg_lambda (1), random_state (42), n_jobs (-1), Cross-Validation (5-Fold): n_splits (5), shuffle (True), random_state (42), scoring (R^2, RMSE via "neg_mean_squared_error")
GBM	n_estimators (200), learning_rate (0.2), max_depth (6), subsample (0.8), random_state (42), Cross-Validation (5-Fold): n_splits (5), shuffle (False, default), random_state (None, default), scoring (MSE via "neg_mean_squared_error"
DFNN	n_estimators: (N/A), Input layer: (Dense(312, activation='relu', input shape=(12,))), dropout_1: (Dropout(0.2)), hidden_layer_1: (Dense(156, activation='relu')), dropout_2: (Dropout(0.2)), hidden_layer_2: (Dense(78, activation='relu')), dropout_3: (Dropout(0.15)), output_layer: (Dense(1)), optimizer: (Adam(learning_rate=0.001)), loss: ('mean_squared_error'), metrics: ('mae'),batch_size: (128), epochs: (100 with early_stopping (patience=15, restore_best_weights=True)), validation_split: (0.2), cross_validation: (5-fold with shuffle=True, random_state=42)

3.2. Model Performance Evaluation

The Datasets were randomly selected into training and test sets, with this procedure repeated 100 times to assess model stability. Performance was evaluated using the coefficient of determination R^2, RMSE and MSE with results summarized present in Table 6. The DFNN model consistently outperformed XGBoost and GBM), explaining over 95% of SMDI variance ($R^2 > 0.95$) with low prediction error (< RMSE, < MSE). In comparison, XGBoost and GBM delivered similar and lower performance.

Table 6: Performance of deep learning and machine learning models on training and test datasets for SMDI prediction.

Model	Train Data			Test Data		
	R^2	RMSE	MSE	R^2	RMSE	MSE
XGBoost	0.923	0.386	0.136	0.906	0.405	0.164
GBM	0.940	0.375	0.106	0.920	0.375	0.141
DFNN	0.962	0.261	0.071	0.959	0.278	0.078

3.3. Analyzing the relative Importance of all drought Factors Using the DFNN model.

The DFNN model quantifies the relative importance of each predictor based on its contribution to the model output. As shown in Table 7, SPEI-3 exhibited the highest relative importance (21.17%), followed by SPEI-6 (15.00%) and SPEI-12 (10.81%), indicating that short- to medium-term climatic anomalies exert the strongest influence on drought conditions. Because SMDI was used as the dependent variable, these findings underscore the sensitivity of agricultural drought to water balance variations over these timescales. EDI (8.62%) and PAI (7.96%) also demonstrated considerable importance, highlighting the roles of evaporative demand and precipitation anomalies. Vegetation indices, including VCI (8.09%), VHI (7.94%), and TCI (5.85%), contributed moderately, while precipitation-only indices such as SPI and PCI had relatively low importance, indicating their limited ability to capture soil-moisture variability.

Table 7: Relative Importance of DFNN features percentage

Drought Variables	Relative Importance (%)
Evaporative drought Index, EDI	8.62
Precipitation Anomaly Index, PAI	7.96
Precipitation condition index, PCI	3.02
Three months of SPEI-3	21.17
Six months of SPEI-6	15.00
Twelve months of SPEI-12	10.81
Three months of SPI-3	1.80
Six months of SPI-6	3.41
Twelve months of SPI-12	6.33
Temperature condition index, TCI	5.85
Vegetation condition index, VCI	8.09
Vegetation health index, VHI	7.94

We analyzed the correlation between SMDI and multiple drought indices, as shown in Figure 5. The correlation analysis indicated that significant relationships existed among each index and SMDI, with the strongest association observed between SPEI-3 of 0.56, followed by SPEI-6 of 0.41 and SPEI-12 of 0.29. The correlations of PAI and PCI with SMDI were 0.25 and 0.16, respectively. Precipitation only indices SPI displayed weaker relationships. Vegetation indices (VCI, VHI) and temperature-based TCI showed modest correlations of 0.21, 0.16 and 0.05, respectively. Notably, EDI correlated negatively with SMDI, indicating that higher evaporative demand corresponds to greater soil moisture deficit. These results are consistent with the result of our analysis for relative importance obtained from the DFNN model, reinforcing the identification of dominant indicators for agricultural drought monitoring.

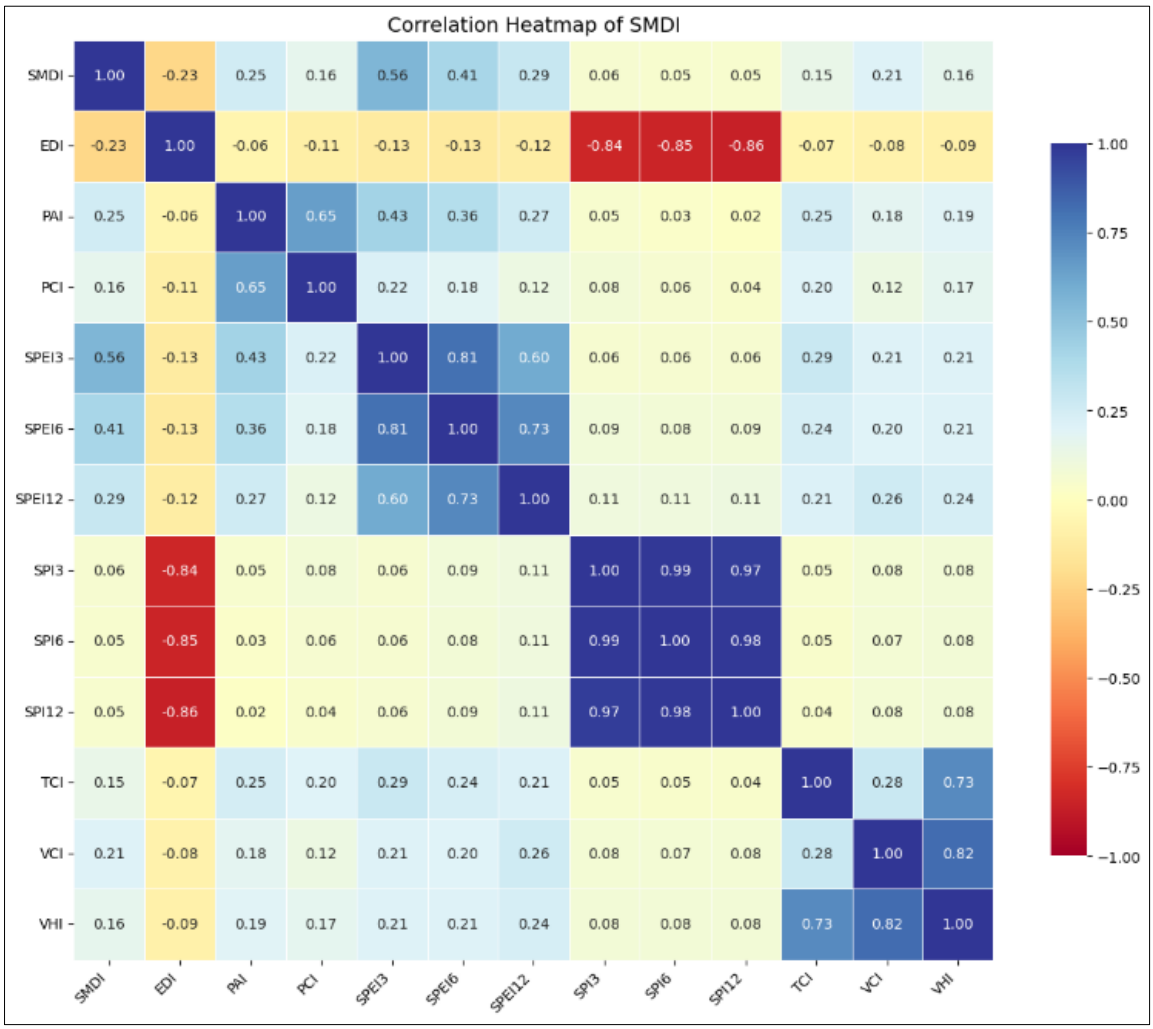

Fig 5: Pearson correlation coefficients matrix of SMDI.

3.4. Simulation of Drought by Spatial Distribution of SMDI in Typical Years

In this study, the average value of SMDI from time-series gridded remote sensing data during the study period was used to obtain the change process of SMDI from 2001 to 2020. It can be seen in Figure 6 that the drought conditions were relatively severe in 2004-2006, 2009, 2011, and 2013. Among these, the droughts hit hardest in 2004 and 2011 the two worst years, while 2005, 2009, and 2013 also exhibited severe drought but with relatively lower intensity compared to the worst years. Additionally, the period from 2014 to 2017 exhibited relatively stable and mild drought conditions. However, drought intensity began to rise again toward the end of the study period, with 2018 and 2019 showing a clear shift to moderate drought. The duration and intensity of drought in other periods followed no obvious patterns. The periods marked by the dashed box in Figure 7 highlight the strongest and longest droughts. These were chosen as typical drought years for detailed spatial mapping.

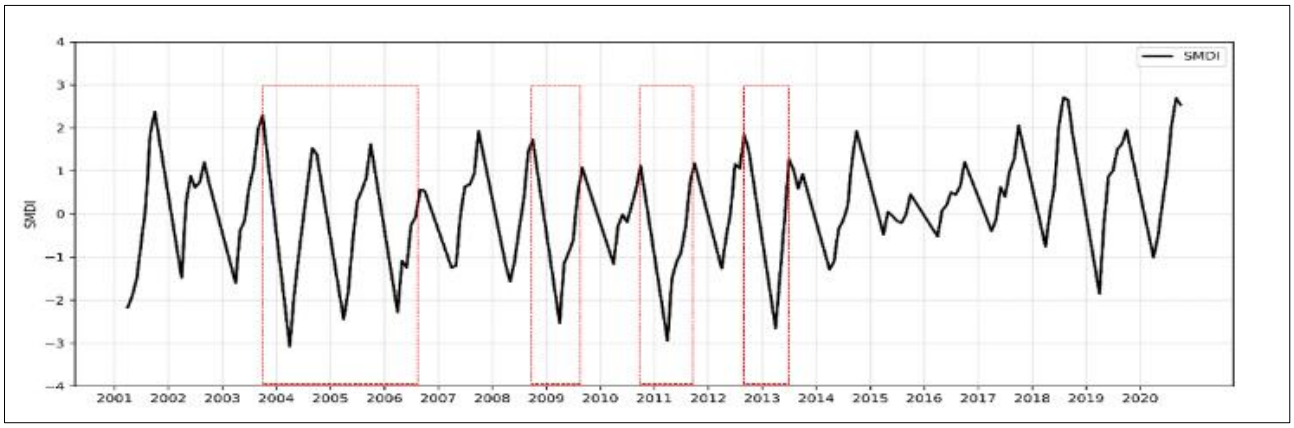

Fig 6: The change of SMDI in Ningxia region during the growing season from 2001-2020.

Using SMDI spatial distribution data and remote sensing time series of SMDI data to evaluate to compare of SMDI spatial distribution the drought monitoring, the typical drought year data 2004, 2005, 2009, 2011 and 2013 were selected and the result are represented in figure 7. In 2004, most of the study area experienced severe drought, with only a small pocket in the southern sector showing mild or negligible drought. In 2005 the pattern was more heterogeneous: the southern half was largely affected by mild drought, while the central and south-central zones exhibited predominantly moderate to severe deficits. The 2009 distribution shows mild drought concentrated in the northernmost areas, whereas central to southwest sectors were characterized by moderate to severe drought. In 2011 drought severity intensified and extended across much of the central, southeastern, and western portions of the region; the north contained isolated patches of mild or no drought. By 2013 the spatial pattern resembled 2011 but with slightly reduced severity moderate to severe drought persisted in the central-southern areas while the northern sector was mostly mild or undisturbed.

However, comparison of SMDI spatial distributions derived from the DFNN simulated and remote-sensing SMDI time series shows strong alignment in both spatial pattern and severity for the typical years. Both datasets consistently identify the central and southern portions of the study area as the most drought-prone, whereas the northern sector tends to be less affected. These concordant results indicate that the DFNN model reliably reproduces the spatial drought characteristics captured by remote-sensing SMDI, supporting its use for spatially explicit monitoring of agricultural drought.

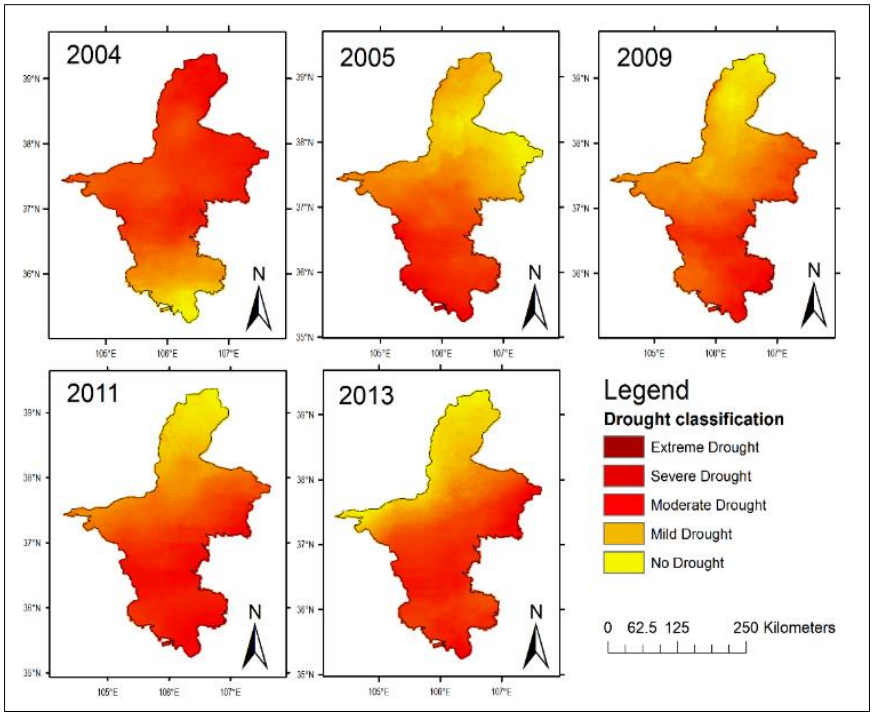

Fig 7: SMDI spatial distribution map simulated by the DFNN model in a typical drought year.

4. Discussion

4.1 Model Performance and Predictive Accuracy

Recent studies have shown that DFNN models often outperform conventional machine learning approaches in agricultural drought monitoring due to their ability to capture complex nonlinear relationships (Gyaneshwar *et al*., 2023) [19]. In this study, we developed a deep learning DFNN model alongside two machine learning models XGBoost and GBM using remote sensing and meteorological data to predict SMDI. The DFNN model outperformed the other two, achieving higher R2 values and lower RMSE and MSE (see Figure 4 and Table 6), consistent with previous findings (Prodhan *et al*., 2021) [36], who demonstrated DFNN superiority for SMDI prediction. Its predictive capability was further validated by comparing time-series SMDI for typical drought years with corresponding spatial distribution maps, which showed coherent temporal and spatial drought patterns similar to those reported in multi-source remote-sensing applications (Y.; Zhang *et al*., 2023) [61]. This superior performance may stem from differences in study area, data sources, model parameters, and input output configurations, as well as DFNN's reduced sensitivity to overfitting and its enhanced ability to model hierarchical and nonlinear interactions among drought influencing variables. These results confirm the effectiveness of DFNN for accurate and robust agricultural drought monitoring across both temporal and spatial scales.

4.2. Relative Importance of Drought Factors Derived from the DFNN Model

In this study, DFNN derived relative importance (Table 6) identified three months of SPEI-3 as the most influential predictor of 21.17%, followed by SPEI-6 (15.00%) and SPEI-12 (10.81%), underscoring the primacy of short- to medium-term anomalies in driving agricultural drought (Vicente-Serrano *et al*., 2010) [47]. EDI (8.62%) and PAI (7.96%) also contributed substantially, highlighting the roles of evaporative demand and precipitation anomalies, respectively. Vegetation indices (VCI, VHI, and TCI) played a moderate role, while precipitation only indices (SPI and PCI) showed lower importance. These findings are consistent with studies demonstrating that vegetation indices

complement meteorological indicators and that SPEI better captures soil moisture variability than SPI alone(Zeng *et al*., 2023) [57]. The Pearson correlation coefficients shown in Fig. 4 mirror this ranking: SPEI-3 (0.56), SPEI-6 (0.41), and SPEI-12 (0.29) exhibit the strongest positive associations with SMDI. In contrast, EDI is negatively correlated with SMDI, reflecting that higher evaporative demand corresponds to greater soil moisture deficit. This negative correlation, despite EDI high model importance, illustrates that DFNN captures nonlinear and predictive contributions, whereas Pearson's r measures only linear associations; thus, EDI serves as an early indicator of atmospheric "thirst" driving soil drying (Hobbins *et al*., 2016) [21]. Overall, these results indicate that SPEI, particularly at the 3-month scale, combined with evaporative demand, represents the dominant indicator for agricultural drought monitoring in the study area (Prodhan *et al*., 2021) [36].

4.3. Spatiotemporal Simulation of Drought Patterns

The combined analysis of SMDI time series and DFNN-simulated spatial fields identifies 2004, 2005, 2009, 2011 and 2013 as the typical drought episodes in Ningxia during 2001–2020, with 2004 and 2011 showing the greatest severity. The prominence of 2004 and the extended dry spell through 2004–2006 reflected in our results is consistent with regional remote-sensing and climatological analyses that record severe vegetation and soil-moisture deficits in the Shaanxi-Gansu-Ningxia corridor during that interval (Tan *et al*., 2015b; Zhao *et al*., 2022) [46, 62]. Our spatial maps further show that 2005 produced a heterogeneous pattern mild drought in parts of the south and moderate-severe deficits in central zones which agrees with TVDI and index-based assessments that flagged 2005 as a major agricultural drought year in Ningxia (Du *et al*., 2017) [12]. The central southern concentration of moderate to severe deficits in 2009 and the extensive, spatially coherent severity observed in 2011 are likewise supported by multi-index regional studies and national drought reports that identify 2010–2011 among the most significant recent dry periods (Zhao *et al*., 2022) [62] national assessments. For 2013, provincial situational reports and peer-reviewed analyses report persistent drought impacts in central southern Ningxia despite localized heavy summer rainfall in the north, a spatial contrast that our SMDI maps reproduce (Fang *et al*., 2018b; *Ningxia Water Resources Department*, 2013) [14, 33].

The strong spatial concordance between DFNN outputs and remote-sensing SMDI supported by the validation analyses presented in the Results (scatterplots, correlation matrix, training/test performance and variable importance; see Results Fig 4, Fig 5, Table 6 and Table 7) provides quantitative confidence in the reproduced drought footprints. Overall, the temporal peaks (Fig. 7) and spatial patterns (Fig. 8) indicate that the DFNN SMDI framework reliably captures the timing and spatial extent of major drought events in study region, supporting its application for spatially explicit agricultural drought monitoring in semi-arid environments.

4.4. Uncertainties and Limitations of this study

Although this study employed one deep learning model (DFNN) and two machine learning models (XGBoost and GBM), along with various drought indices, to estimate SMDI in the study area, the DFNN framework demonstrated high predictive accuracy and strong agreement between observed and predicted temporal and spatial drought patterns, several uncertainties remain. Model reliability depends on the precision and consistency of input datasets, as both remote sensing and meteorological observations are subject to retrieval noise, spatial averaging, and sensor calibration errors that can propagate into the drought indices (Du *et al*., 2017; Y.; Zhang *et al*., 2023) [12, 61]. The use of 1-km spatial resolution data provides robust regional coverage but may not fully resolve fine-scale soil moisture variability or vegetation stress across heterogeneous landscapes, particularly in southern Ningxia. Additionally, reliance on annual growing-season data may obscure short-term drought fluctuations and transitional phases between wet and dry periods. Uncertainties also stem from the inherent black-box nature of DFNN models. Although feature importance analysis provides interpretive insights, the internal nonlinear interactions remain complex and not fully transparent (Gyaneshwar *et al*., 2023) [19]. Moreover, validation was based primarily on remotely sensed SMDI, which, despite being well established, remains an indirect proxy for actual soil moisture. Future research should integrate multi-source datasets with higher temporal resolution and adopt interpretable deep learning frameworks to enhance transparency, generalization, and robustness in agricultural drought monitoring.

5. Conclusion

This present study, a deep learning DFNN framework was developed to monitor agricultural drought across the arid and semi-arid Ningxia region during the growing seasons from 2001 to 2020. By integrating twelve drought indices derived from remote sensing and meteorological data, the DFNN effectively captured nonlinear interactions among precipitation, vegetation and soil moisture as represented by the SMDI. The model achieved strong predictive performance with a test R^2 of 0.95, outperforming XGBoost and GBM, and accurately reproduced the spatial and temporal variability of drought across the region. The analysis identified the three-month SPEI-3 as the most influential predictor, followed by the EDI, underscoring their dominant roles in driving agricultural drought conditions. Vegetation based indices (VC, TCI, VHI) contributed moderately, reflecting delayed vegetation responses to moisture stress. The DFNN successfully identified key on typical drought years 2004, 2005, 2009, 2011, and 2013 demonstrating strong alignment between time series remote sensing derived SMDI trends and the spatial distribution of drought severity. Overall, the DFNN based approach proved to be a reliable and scalable data-driven framework for agricultural drought monitoring in semi-arid regions. By effectively integrating multisource environmental information and validating results through both temporal and spatial SMDI analyses, this study provides a robust foundation for operational drought assessment. Future work should focus on incorporating higher-temporal-resolution satellite data and applying explainable deep learning methods to enhance interpretability and real-time forecasting capabilities

6. Acknowledgement

This work was supported by the Central Guiding Local Science and Technology Development Fund of Shandong Yellow River Basin Collaborative Science and Technology Innovation Special Project (No. YDZX2023019), Shandong Provincial Natural Science Foundation (ZR2023QD073; No.

ZR2020QE281; No. ZR2024LQX005).

Authors' Contributions: Khandakar Md Bappy: data curation, investigation, software, methodology, Formal analysis, writing—original draft preparation. Ali Shahzad: formal analysis, validation, writing—review and editing. Abdul Basit: formal analysis, validation, writing—review and editing. Shawkat Ali : writing—review and editing; Hidayat Ullah: review and editing; Muhammad Awais; review and editing: Zakria Zaheen writing; review and editing; Jiahua Zhang: Supervise and writing—review; Kalisa Wilson : funding acquisition, project administration, writing—review. All authors have read and agreed to the published version of the manuscript.

Competing Interests: The authors declare that they have no known competing financial interests or personal relationships that could have appeared to influence the work reported in this paper

7. References

1. Abadi M, Agarwal A, Barham P, Brevdo E, Chen Z, Citro C, *et al*. TensorFlow: large-scale machine learning on heterogeneous distributed systems. 2016. Available from: https://arxiv.org/pdf/1603.04467
2. AghaKouchak A, Farahmand A, Melton FS, Teixeira J, Anderson MC, Wardlow BD, *et al*. Remote sensing of drought: progress, challenges and opportunities. Rev Geophys. 2015;53(2):452–80. doi:10.1002/2014RG000456
3. Beguería S, Vicente-Serrano SM, Reig F, Latorre B. Standardized precipitation evapotranspiration index (SPEI) revisited: parameter fitting, evapotranspiration models, tools, datasets and drought monitoring. Int J Climatol. 2014;34(10):3001–23. doi:10.1002/joc.3887
4. Britannica. Ningxia: land, people, economy, history, & facts [Internet]. [place unknown: publisher unknown]; [date unknown] [cited 2025 Oct 14]. Available from: https://www.britannica.com/place/Ningxia?utm_source=chatgpt.com
5. Chen H, Liang Z, Liu Y, Jiang Q, Xie S. Effects of drought and flood on crop production in China across 1949-2015: spatial heterogeneity analysis with Bayesian hierarchical modeling. Nat Hazards. 2018;92:525–41. doi:10.1007/s11069-018
6. Chen H, Sun J. Changes in drought characteristics over China using the Standardized Precipitation Evapotranspiration Index. J Clim. 2015;28(13):5430–47. doi:10.1175/JCLI-D-14-00707.1
7. Chen T, Guestrin C. XGBoost: a scalable tree boosting system. In: Proceedings of the ACM SIGKDD International Conference on Knowledge Discovery and Data Mining; 2016 Aug 13-17. p. 785–94. doi:10.1145/2939672.2939785
8. Chen Z, Huang M, Xiao C, Qi S, Du W, Zhu D, *et al*. Integrating remote sensing and spatiotemporal analysis to characterize artificial vegetation restoration suitability in desert areas: a case study of Mu Us Sandy Land. Remote Sens. 2022;14(19):4736. doi:10.3390/rs14194736
9. Chollet F. Keras high-level API for building/training DFNNs [Internet]. 2015 [cited 2025 Oct 14]. Available from: https://keras.io
10. Didan K. MOD13Q1 MODIS/Terra vegetation indices 16-day L3 global 250m SIN grid V006 [Internet]. NASA EOSDIS Land Processes DAAC; 2015 [cited 2025 Oct 14]. Available from: [no URL provided in original]
11. Du L, Gong F, Zeng Y, Ma L, Qiao C, Wu H. Carbon use efficiency of terrestrial ecosystems in desert/grassland biome transition zone: a case in Ningxia province, northwest China. Ecol Indic. 2021;120:106971. doi:10.1016/j.ecolind.2020.106971
12. Du L, Song N, Liu K, Hou J, Hu Y, Zhu Y, *et al*. Comparison of two simulation methods of the temperature vegetation dryness index (TVDI) for drought monitoring in semi-arid regions of China. Remote Sens. 2017;9(2):177. doi:10.3390/rs9020177
13. Duan Y, Bo Y, Yao X, Chen G, Liu K, Wang S, *et al*. A deep learning framework for long-term soil moisture-based drought assessment across the major basins in China. Remote Sens. 2025;17(6):1000. doi:10.3390/rs17061000
14. Fang Y, Qian H, Chen J, Xu H. Characteristics of spatial-temporal evolution of meteorological drought in the Ningxia Hui Autonomous Region of northwest China. Water. 2018;10(8):992. doi:10.3390/w10080992
15. Kogan FN. Global drought watch from space. Bull Am Meteorol Soc. 1997;78:621–36.
16. Friedman JH. Greedy function approximation: a gradient boosting machine. Ann Stat. 2001;29(5):1189–232. doi:10.1214/aos/1013203451
17. Funk C, Peterson P, Landsfeld M, Pedreros D, Verdin J, Shukla S, *et al*. The climate hazards infrared precipitation with stations—a new environmental record for monitoring extremes. Sci Data. 2015;2(1):150066. doi:10.1038/sdata.2015.66
18. Gao F, Zhang Y, Ren X, Yao Y, Hao Z, Cai W. Evaluation of CHIRPS and its application for drought monitoring over the Haihe River Basin, China. Nat Hazards. 2018;92(1):155–72. doi:10.1007/s11069-018-3196-0
19. Gyaneshwar A, Mishra A, Chadha U, Raj Vincent PMD, Rajinikanth V, Pattukandan Ganapathy G, *et al*. A contemporary review on deep learning models for drought prediction. Sustainability. 2023;15(7):6160. doi:10.3390/su15076160
20. Hanadé Houmma I, El Mansouri L, Gadal S, Garba M, Hadria R. Modelling agricultural drought: a review of latest advances in big data technologies. Geomatics Nat Hazards Risk. 2022;13(1):2737–76. doi:10.1080/19475705.2022.2131471
21. Hobbins MT, Wood A, McEvoy DJ, Huntington JL, Morton C, Anderson M, *et al*. The evaporative demand drought index. Part I: linking drought evolution to variations in evaporative demand. J Hydrometeorol. 2016;17(6):1745–61. doi:10.1175/JHM-D-15-0121.1
22. Goodfellow I, Courville A, Bengio Y. Deep learning. Adaptive computation and machine learning series. Cambridge (MA): MIT Press; 2016. p. 1–23. Available from: http://www.deeplearningbook.org
23. Jiao W, Zhang L, Chang Q, Fu D, Cen Y, Tong Q. Evaluating an enhanced vegetation condition index (VCI) based on VIUPD for drought monitoring in the continental United States. Remote Sens. 2016;8(3):224. doi:10.3390/rs8030224
24. Justice CO, Townshend JRG, Vermote EF, Masuoka E, Wolfe RE, Saleous N, *et al*. An overview of MODIS land

data processing and product status. Remote Sens Environ. 2002;83(1-2):3–15. doi:10.1016/S0034-4257(02)00084-6
25. Kogan FN. Application of vegetation index and brightness temperature for drought detection. Adv Space Res. 1995;15(11):91–100. doi:10.1016/0273-1177(95)00079-T
26. Kogan FN. Satellite-observed sensitivity of world land ecosystems to El Niño/La Niña. Remote Sens Environ. 2000;74(3):445–62. doi:10.1016/S0034-4257(00)00137-1
27. Li C, Fu B, Wang S, Stringer LC, Wang Y, Li Z, *et al*. Drivers and impacts of changes in China's drylands. Nat Rev Earth Environ. 2021;2(12):858–73. doi:10.1038/s43017-021-00226-z
28. Li X, Tan J, Wang X, Shang Q, Li H, Li X. Analysis of future drought risk and wheat meteorological disaster in Ningxia (northwest China) based on CMIP6 and SPEI. Agronomy. 2024;14(12):3051. doi:10.3390/agronomy14123051
29. McKee TB, Doesken NJ, Kleist J. The relationship of drought frequency and duration to time scales. In: Eighth Conference on Applied Climatology; 1993 Jan 17-22; Anaheim (CA).
30. Meng J, Yang X, Li Z, Zhao G, He P, Xuan Y, *et al*. Tracking evapotranspiration patterns on the Yinchuan Plain with multispectral remote sensing. Sustainability. 2024;16(18):8025. doi:10.3390/su16188025
31. Mishra AK, Singh VP. A review of drought concepts. J Hydrol. 2010;391(1-2):202–16. doi:10.1016/j.jhydrol.2010.07.012
32. Narasimhan B, Srinivasan R. Development and evaluation of soil moisture deficit index (SMDI) and evapotranspiration deficit index (ETDI) for agricultural drought monitoring. Agric For Meteorol. 2005;133(1-4):69–88. doi:10.1016/j.agrformet.2005.07.012
33. Ningxia Water Resources Department. Ningxia water resources bulletin [Internet]. 2013 [cited 2025 Oct 14]. Available from: https://slt.nx.gov.cn/
34. Park S, Im J, Jang E, Rhee J. Drought assessment and monitoring through blending of multi-sensor indices using machine learning approaches for different climate regions. Agric For Meteorol. 2016;216:157–69. doi:10.1016/j.agrformet.2015.10.011
35. Prodhan FA, Zhang J, Hasan SS, Pangali Sharma TP, Mohana HP. A review of machine learning methods for drought hazard monitoring and forecasting: current research trends, challenges, and future research directions. Environ Model Softw. 2022;149:105327. doi:10.1016/j.envsoft.2022.105327
36. Prodhan FA, Zhang J, Yao F, Shi L, Sharma TPP, Zhang D, *et al*. Deep learning for monitoring agricultural drought in South Asia using remote sensing data. Remote Sens. 2021;13(9):1715. doi:10.3390/rs13091715
37. Quiring SM. Developing objective operational definitions for monitoring drought. J Appl Meteorol Climatol. 2009;48(6):1217–29. doi:10.1175/2009JAMC2088.1
38. Reichstein M, Camps-Valls G, Stevens B, Jung M, Denzler J, Carvalhais N, *et al*. Deep learning and process understanding for data-driven Earth system science. Nature. 2019;566(7743):195–204. doi:10.1038/s41586-019-0912-1
39. Rodell M, Houser PR, Jambor U, Gottschalck J, Mitchell K, Meng CJ, *et al*. The global land data assimilation system. Bull Am Meteorol Soc. 2004;85(3):381–94. doi:10.1175/BAMS-85-3-381
40. Shen C. A transdisciplinary review of deep learning research and its relevance for water resources scientists. Water Resour Res. 2018;54(11):8558–93. doi:10.1029/2018WR022643
41. Shen R, Huang A, Li B, Guo J. Construction of a drought monitoring model using deep learning based on multi-source remote sensing data. Int J Appl Earth Obs Geoinf. 2019;79:48–57. doi:10.1016/j.jag.2019.03.006
42. Shi X, Ding H, Wu M, Shi M, Chen F, Li Y, *et al*. A comprehensive drought monitoring method integrating multi-source data. PeerJ. 2022;10:e13560. doi:10.7717/peerj.13560
43. SPEIbase v2.10. Standardised Precipitation-Evapotranspiration Index database, version 2.10 [Internet]. Spanish National Research Council (CSIC); [date unknown] [cited 2025 Oct 14]. Available from: [no URL provided in original]
44. Sun H, Xu Q, Wang Y, Zhao Z, Zhang X, Liu H, *et al*. Agricultural drought dynamics in China during 1982–2020: a depiction with satellite remotely sensed soil moisture. GISci Remote Sens. 2023;60(1):2257469. doi:10.1080/15481603.2023.2257469
45. Svoboda M, LeComte D, Hayes M, Heim R, Gleason K, Angel J, *et al*. The drought monitor. Bull Am Meteorol Soc. 2002;83(8):1181–90. doi:10.1175/1520-0477-83.8.1181
46. Tan C, Yang J, Li M. Temporal-spatial variation of drought indicated by SPI and SPEI in Ningxia Hui Autonomous Region, China. Atmosphere. 2015;6(10):1399–421. doi:10.3390/atmos6101399
47. Vicente-Serrano SM, Beguería S, López-Moreno JI. A multiscalar drought index sensitive to global warming: the Standardized Precipitation Evapotranspiration Index. J Clim. 2010;23(7):1696–718. doi:10.1175/2009JCLI2909.1
48. Wan Z. MOD11A2 MODIS/Terra land surface temperature/emissivity 8-day L3 global 1km SIN grid V006 [Internet]. NASA EOSDIS Land Processes DAAC; 2015 [cited 2025 Oct 14]. Available from: [no URL provided in original]
49. Wang Q, Zhao L, Wang M, Wu J, Zhou W, Zhang Q, *et al*. A random forest model for drought: monitoring and validation for grassland drought based on multi-source remote sensing data. Remote Sens. 2022;14(19):4981. doi:10.3390/rs14194981
50. Wilhite DA, Glantz MH. Understanding the drought phenomenon: the role of definitions [Internet]. Lincoln (NE): University of Nebraska-Lincoln Digital Commons; 1985 [cited 2025 Oct 14]. Available from: http://digitalcommons.unl.edu/droughtfacpub/20
51. Xu Z, Sun H, Zhang T, Xu H, Wu D, Gao JH. Evaluating established deep learning methods in constructing integrated remote sensing drought index: a case study in China. Agric Water Manag. 2023;286:108405. doi:10.1016/j.agwat.2023.108405
52. Yan N, Wu B, Zhu W, Ma Z, Zhang X, Bulgan D. The evolution of irrigation effects on agricultural drought mitigation in North China. Remote Sens. 2022;14(20):5197. doi:10.3390/rs14205197
53. Yang J, Tan C, Wang S, Wang S, Yang Y, Chen H.

Drought adaptation in the Ningxia Hui Autonomous Region, China: actions, planning, pathways and barriers. Sustainability. 2015;7(11):15029–56. doi:10.3390/su71115029
54. Yang P, Zhai X, Huang H, Zhang Y, Zhu Y, Shi X, *et al*. Association and driving factors of meteorological drought and agricultural drought in Ningxia, northwest China. Atmos Res. 2023;289:106753. doi:10.1016/j.atmosres.2023.106753
55. Yao Y, Liang S, Qin Q, Wang K. Monitoring drought over the conterminous United States using MODIS and NCEP Reanalysis-2 data. J Appl Meteorol Climatol. 2010;49(8):1665–80. doi:10.1175/2010JAMC2328.1
56. Yao Y, Liang S, Qin Q, Wang K, Zhao S. Monitoring global land surface drought based on a hybrid evapotranspiration model. Int J Appl Earth Obs Geoinf. 2011;13(3):447–57. doi:10.1016/j.jag.2010.09.009
57. Zeng J, Zhou T, Qu Y, Bento VA, Qi J, Xu Y, *et al*. An improved global vegetation health index dataset in detecting vegetation drought. Sci Data. 2023;10(1):338. doi:10.1038/s41597-023-02255-3
58. Zhang A, Jia G, Wang H. Improving meteorological drought monitoring capability over tropical and subtropical water-limited ecosystems: evaluation and ensemble of the Microwave Integrated Drought Index. Environ Res Lett. 2019;14(4):044025. doi:10.1088/1748-9326/ab005e
59. Zhang H, Wang Z, Shang G, Huang Y, Li H, Ding X, *et al*. Analysis of the evolution pattern and driving mechanism of lakes in the northern Ningxia Yellow Diversion Irrigation Area. Water. 2022;14(22):3658. doi:10.3390/w14223658
60. Zhang L, Yao Y, Bei X, Jia K, Zhang X, Xie X, *et al*. Assessing the remotely sensed evaporative drought index for drought monitoring over Northeast China. Remote Sens. 2019;11(17):1960. doi:10.3390/rs11171960
61. Zhang Y, Xie D, Tian W, Zhao H, Geng S, Lu H, *et al*. Construction of an integrated drought monitoring model based on deep learning algorithms. Remote Sens. 2023;15(3):667. doi:10.3390/rs15030667
62. Zhao X, Xia H, Liu B, Jiao W. Spatiotemporal comparison of drought in Shaanxi–Gansu–Ningxia from 2003 to 2020 using various drought indices in Google Earth Engine. Remote Sens. 2022;14(7):1570. doi:10.3390/rs14071570

How to Cite This Article

Khandakar Md Bappy, Shahzad A, Basit A, Ali S, Ullah H, Awais M, Zaheen Z, Wilson K, Zhang J. Monitoring agricultural drought in Ningxia region of China using remote sensing data and deep learning model. Int J Adv Inf Eng Technol. 2025;6(2):49–63. doi:10.54660/IJAIET.2025.6.2.49-63.

Creative Commons (CC) License